Magneto-Structural Characterization of Oxalamide Dihalo-Bridged Copper Dimers: Intra- and Interdimer Interactions Studied by Single Crystal ESR Spectroscopy

Dijana Žilić,[*,†] Debdeep Maity,[†] Mario Cetina,[‡] Zoran Džolić,[†] and Mirta Herak[*,¶]

†*Ruđer Bošković Institute, Bijenička c. 54, HR-10000, Croatia.*

‡*University of Zagreb, Faculty of Textile Technology, Department of Applied Chemistry, Prilaz baruna Filipovića 28a, HR-10000 Zagreb, Croatia.*

¶*Institute of Physics, Bijenička c. 46, HR-10000 Zagreb, Croatia.*

E-mail: dzilic@irb.hr; mirta@ifs.hr

Abstract

The detailed single crystal electron spin resonance (ESR) analysis of oxalamide complexes with halogen-bridged copper dimers, supported by X-ray, magnetic susceptibility and powder ESR studies, is reported. Four complexes with two different ligands were synthesized: $[CuL^A(\mu\text{-X})]_2$ and $[CuL^V(\mu\text{-X})]_2$, where L^A = *N*-(L-alanine methyl ester)-*N'*-((2-pyridine-2-yl)methyl)oxalamide and L^V=*N*-(L-valine methyl ester)-*N'*-((2-pyridine-2-yl)methyl)oxalamide, while X=Cl or Br. X-ray structural analysis shows that geometry at each copper(II) ion is ideal or near ideal square pyramidal while two pyramids share one base-to-apex edge with parallel basal planes. The complexes are linked by hydrogen bonds into infinite chains, which are further linked into a three-dimensional network. Magnetic susceptibility measurements show that coppers in dimers are weakly antiferromagnetically coupled ($|J| \approx 0.6 - 3$ K). From powder ESR experiments, *g*-values and $d_{x^2-y^2}$ orbital as the ground state of unpaired electron are determined, in agreement with copper square-bipyramide structures. Despite very similar structures of these complexes compared with the complexes previously reported and characterized by similar X-ray, magnetization and powder ESR results, single crystal ESR spectra reveal significant differences.[Žilić D. et al., *Dalton Trans.* **2014**, *43*, 11877–11887] Here presented complexes show unusual anisotropic splitting and merging of ESR lines when their crystals rotate in magnetic field. The observation of this partially resolved intradimer dipolar splitting enabled estimation of weak interdimer exchange interaction parameter $|J'| \sim 1$ mK.

Introduction

The characterization of exchange-coupled transition metal complexes has become a multidisciplinary research field with application in physics, chemistry and biology. The information obtained from these studies is important for design of new materials with predictable magnetic properties and molecule-based magnets,[1–3] as well as to understand electron-transfer reactions in protein.[4–6] Study of dinuclear copper(II) complexes, as the simplest coupled magnetic systems with $S = 1/2$ spin pair, has essential role in the field of molecular magnetism[7] and a lot of effort has been put into investigation of magnetic properties in the light of their relation to structural features.[8–11] Generally, in dinuclear compounds, spin-spin interaction is determined by isotropic exchange constant, J, and by anisotropic interactions such as symmetric anisotropic and antisymmetric Dzyaloshinskii-Moriya exchange and dipolar magnetic coupling.[1,7] Isotropic exchange interaction separates the singlet from the triplet state by an energy J while anisotropic interactions remove the degeneracy of the triplet state even in zero magnetic field. In copper complexes, also important is hyperfine interaction, due to coupling of electron spin $S = 1/2$ with the spin of copper nucleus $I = 3/2$. Furthermore, in undiluted magnetic systems, dimers may interact via weak exchange interaction J' through different chemical paths which introduces another complexity into magnetic structure.[12]

Recently, magneto-structural correlations in a set of dihalo-bridged oxalamide copper(II) dimers were reported.[13] Here presented four newly synthesized complexes have slightly different ligands compared to those previously reported. Standard crystallographic, magnetic susceptibility and powder ESR characterization of both type of complexes were performed and, as it is expected, similar results were obtained. Copper(II) ions, with almost ideal square pyramidal geometry, are weakly antiferromagnetically coupled ($|J| \approx 1$ K) in dimers. The dimers are further linked by hydrogen bonds into chains and three-dimensional networks. However, performing single crystal ESR spectroscopy, during crystal rotation in magnetic field, significantly different spectra were obtained. While for $Z = 1$ for the previously reported complexes, only single ESR line was always detected, here presented complexes show

unusual partially resolved anisotropic line splitting. Exploiting the phenomena of exchange narrowing and collapse or merging of split lines,[7,12,14–25] we assign this splitting to intradimer dipolar interaction. Furthermore, applying the model introduced by Hoffmann and coworkers,[15–17,22,26,27] we were able to estimate exchange interaction between dimers J'. Therefore, when studying this type of compounds, single crystal ESR spectroscopy has proven to be particularly useful experimental technique due to its sensitivity to probe small difference in weak intra- and interdimer interactions.[7,12,14–19]

Experimental methods

Synthesis and characterization of compounds

The ligands prepared from L-valine and L-alanine, as well as corresponding Cu complexes, were synthesized as previously described.[13,28] Reagents were purchased from Aldrich or Fluka and were used without further purification. All solvents were purified and dried by using standard procedures and distilled prior to use. Melting points were determined on a Kofler hot-stage apparatus and are uncorrected. ^{1}H and ^{13}C NMR spectra were recorded on a Bruker AV 300 spectrometer. Chemical shifts (in ppm) are referenced to TMS as an internal standard. Optical rotations were measured on an Optical Activity AA-10 Automatic Polarimeter in a cell (path length: 1 dm) at 589 nm; concentrations are given in g/100 mL. Single-reflection attenuated total reflection (SR-ATR) FT-IR spectra were recorded at a resolution of 4 cm^{-1} on an ABBBomem MB102 single beam FT-IR spectrometer that was equipped with CsI optics and a DTGS detector for a total of 30 scans by using a horizontal single-reflection ATR diamond prism with a 458 angle of incidence. Each spectrum was recorded as the ratio of the sample spectrum to the spectrum of the empty ATR plate.

Ligand $\mathbf{L^A}$ Yield: 64%; m.p.: 98°C; α_D^{20}: - 37 (c=1 in DMSO); IR (KBr): λ =3288, 1754, 1744, 1650, 1523, 1432 cm^{-1}; ^{1}H NMR (DMSO-d_6): δ/ppm = 9.29 (t, J = 6.0 Hz, 1H, -CH$_2$*NH*), 9.10 (d, J = 7.7 Hz, 1H, -CH*NH*CO), 8.50 (dd, J = 5.1 and 1.8 Hz, 1H, C-H$_{aryl}$),

7.76 (t, J = 7.7 Hz, 1H, C-H$_{aryl}$), 7.27 (m, 2H, CH$_{aryl}$), 4.42 (m, 3H, -CH$_\alpha$, CH_2NH), 3.65 (s, 3H, -OCH3), 1.37 (d, J = 7.3 Hz, 3H, -CH3); ^{13}C NMR (DMSO-d_6): δ/ppm =172.4, 160.2, 160.1, 157.8, 149.3, 137.2, 122.7, 121.4, 52.5, 48.3, 44.6, 16.9. Elemental analysis: calcd for $C_{12}H_{15}N_3O_4$ = C 54.34; H 5.70; N 15.84. Found = C 54.29; H 5.72; N 15.81.

Ligand $\mathbf{L^V}$ Yield: 68%; m.p.:92°C; α_D^{20}: - 30 (c = 1 in DMSO); IR (KBr): λ =3272, 2957, 1739, 1652, 1516, 1435 cm^{-1}; ^{1}H NMR (DMSO-d_6): δ/ppm =9.36 (t, J = 6.0 Hz, 1H, -CH$_2$$NH$), 8.69 (d, J = 8.4 Hz, 1H, -CHNHCO), 8.51 (m, 1H, C-H$_{aryl}$), 7.76 (t, J = 7.8 Hz, 1H, C-H$_{aryl}$), 7.27 (m, 2H, C-H$_{aryl}$), 4.46 (t, J = 5.4 Hz, 2H, -CH_2NH), 4.18 (t, J = 7.8, -CH$_\alpha$), 3.66 (s, 3H, -OCH$_3$), 2.21 (m, 1H, CH$_\beta$), 0.88 (dd, J = 6.6 and 3.6 Hz, 6H, 2 x CH3); ^{13}C NMR (DMSO-d_6):δ/ppm =171.0, 160.0, 159.6, 157.2, 148.9, 136.7, 122.2, 121.0, 57.9, 51.9, 44.2, 29.5, 18.9, 18.4. Elemental analysis: calcd for $C_{12}H_{15}N_3O_4$ = C 57.33; H 6.53; N 14.32. Found = C 57.40; H 6.52; N 14.35.

[CuL^A(μ-Cl)]$_2$ Elemental analysis: calcd for $C_{24}H_{28}Cl_2Cu_2N_6O_8$ = C 39.68; H 3.88; N 11.57; Cu 17.49. Found = C 39.72; H 3.90; N 11.54; Cu 17.47. IR (KBr): λ =3212, 3190, 2950, 1745, 1612, 1543 cm^{-1}.

[CuL^A(μ-Br)]$_2$ Elemental analysis: calcd for $C_{24}H_{28}Br_2Cu_2N_6O_8$ = C 35.35; H 3.46; N 10.30; Cu 15.59. Found = C 35.29; H 3.50; N 10.34; Cu 17.40.IR (KBr): λ =3210, 3193, 3071, 1743, 1672, 1610, 1427 cm^{-1}.

[CuL^V(μ-Cl)]$_2$ Elemental analysis: calcd for $C_{28}H_{36}Cl_2Cu_2N_6O_8$ = C 42.98; H 4.64; N 10.74; Cu 16.24. Found = C 42.93; H 4.71; N 10.79; Cu 16.26.IR (KBr): λ =3208, 3189, 3075, 1750, 1739, 1658, 1562 cm^{-1}.

[CuL^V(μ-Br)]$_2$ Elemental analysis: calcd for $C_{28}H_{36}Br_2Cu_2N_6O_8$ = C 38.59; H 4.16; N 9.64; Cu 14.58. Found = C 38.663; H 4.01; N 9.70; Cu 14.59.IR (KBr): λ =3187, 3071, 1752, 1737, 1661, 1566, 1430 cm^{-1}.

Crystal structure determination

Single crystals suitable for X-ray single crystal structure analysis of all complexes were obtained at room temperature by partial evaporation from methanol solution. Data for $[CuL^{A}(\mu\text{-Cl})]_2$ and $[CuL^{A}(\mu\text{-Br})]_2$ were collected at 295 K on Oxford Diffraction Xcalibur Nova R diffractometer with Ruby detector using mirror-monochromatized CuK_α radiation ($\lambda = 1.54184$ Å). Data for $[CuL^{V}(\mu\text{-Cl})]_2$ and $[CuL^{V}(\mu\text{-Br})]_2$ were collected at the same temperature on Oxford Diffraction Xcalibur2 diffractometer with Sapphire 3 CCD detector using graphite-monochromatized MoK_α radiation ($\lambda = 0.71073$ Å). *CrysAlis PRO* program[29] was used for the data collection and processing. For $[CuL^{A}(\mu\text{-Cl})]_2$, $[CuL^{A}(\mu\text{-Br})]_2$ and $[CuL^{V}(\mu\text{-Cl})]_2$, the intensities were corrected for absorption using the multi-scan absorption correction method, while for $[CuL^{V}(\mu\text{-Br})]_2$ numerical absorption correction method was applied.[29] Although the best absorption model was used, higher absorption in two bromide complexes $[CuL^{A}(\mu\text{-Br})]_2$ and $[CuL^{V}(\mu\text{-Br})]_2$, as well as thermal motions resulted in checkCIF B level alert (low bond precision on C–C bonds). The structures were solved using direct methods with *SHELXS-2013*[30] ($[CuL^{A}(\mu\text{-Cl})]_2$, $[CuL^{V}(\mu\text{-Cl})]_2$ and $[CuL^{V}(\mu\text{-Br})]_2$) and *SIR-2004*[31] ($[CuL^{A}(\mu\text{-Br})]_2$), and were refined by full-matrix least-squares calculations based on F^2 using *SHELXL-2014*[30] integrated in the *WinGX*[32] program package. Hydrogen atoms attached to the N3 and N6 atoms in $[CuL^{A}(\mu\text{-Cl})]_2$, $[CuL^{V}(\mu\text{-Cl})]_2$ and $[CuL^{V}(\mu\text{-Br})]_2$ have been found in Fourier maps, and have been refined with geometric restraint on N–H distance (N–H = 0.86 Å). All other hydrogen atoms in these three structures, as well as in $[CuL^{A}(\mu\text{-Br})]_2$, were included in calculated positions with *SHELXL-2014*[30] defaults. The O3A atom in $[CuL^{A}(\mu\text{-Br})]_2$ was disordered over two sites and was refined with fixed occupancy ratio of 0.52/0.48. Restraint on anisotropic thermal parameters was applied in the refinement of these two components, as well as on some carboxylate ester atoms (C13B, C25B, O8B), while geometric restraint was applied in the refinement of C12A–O3A and C12A–O3A' bonds. Restraint on anisotropic displacement parameters was also applied in the refinement of the carbonyl O3 atom in $[CuL^{A}(\mu\text{-Cl})]_2$, as well as valine moiety C26 atom in $[CuL^{V}(\mu\text{-Cl})]_2$ and

C11 and C13 atoms in $[CuL^{V}(\mu\text{-Br})]_2$. Structure of $[CuL^{A}(\mu\text{-Cl})]_2$ contains solvent accessible voids with very small amount of methanol molecule used for recrystallization or water molecule. As it could not be modelled satisfactorily data were treated with the *Squeeze* routine in *PLATON.*[33] Refinement was done in accord with suggested procedure[34] (response to CheckCIF B level Alert). Details of crystal data, data collection, and refinement parameters are given in Table 1. The *PLATON*[33] and *MERCURY*[35] programs were used for structure analysis and molecular and crystal structure drawings preparation. The CCDC 1521402-1521405 contain the supplementary crystallographic data for this paper. These data can be obtained free of charge from The Cambridge Crystallographic Data Centre via *www.ccdc.cam.ac.uk/data_request/cif*.

Table 1: X-ray crystallographic Data for Complexes Described in This Work

Structure	$[\mathbf{CuL^{A}}(\mu\text{-Cl})]_2$	$[\mathbf{CuL^{A}}(\mu\text{-Br})]_2$	$[\mathbf{CuL^{V}}(\mu\text{-Cl})]_2$	$[\mathbf{CuL^{V}}(\mu\text{-Br})]_2$
Formula	$C_{24}H_{28}Cl_2Cu_2N_6O_8$	$C_{24}H_{28}Br_2Cu_2N_6O_8$	$C_{28}H_{36}Cl_2Cu_2N_6O_8$	$C_{28}H_{36}Br_2Cu_2N_6O_8$
Formula weight	726.50	815.42	782.61	871.53
T (K)	295	295	295	295
Radiation, λ (Å)	CuK_α, 1.54184	CuK_α, 1.54184	MoK_α, 0.71073	MoK_α, 0.71073
Crystal system	Monoclinic	Triclinic	Triclinic	Triclinic
Space group	$P2_1$	$P\bar{1}$	$P\bar{1}$	$P\bar{1}$
Unit cell dimensions				
a (Å)	8.0681(3)	9.7483(2)	8.2233(4)	8.3218(5)
b (Å)	18.0851(10)	12.6740(5)	10.3024(5)	10.2781(6)
c (Å)	10.8021(5)	13.7659(6)	11.5787(6)	11.5581(7)
α (°)	90	116.966(4)	114.857(5)	114.297(6)
β (°)	95.281(4)	90.858(3)	101.567(4)	101.275(5)
γ (°)	90	94.831(2)	95.286(4)	94.964(5)
V (Å^3)	1569.47(13)	1507.77(11)	854.65(8)	868.08(10)
Z	2	2	1	1
D_{calc} (g cm^{-3})	1.537	1.796	1.521	1.667
Absorption coef. μ (mm^{-1})	3.704	5.331	1.455	3.581
Θ range (°)	4.110–69.991	3.609–69.978	4.449–29.996	4.429–29.992
Collected reflections No.	7294	13360	17946	17820
Independent reflections No. /$R_{Int.}$	4801 / 0.0191	6649 / 0.0395	9902 / 0.0261	10070 / 0.0274
Reflections No. $I > 2\sigma(I)$	4573	6259	7643	7445
Data[a] /Restraints/Parameters	4801 / 9 / 388	6649 / 35 / 775	9902 / 11 / 430	10070 / 17 / 427
Flack parameter, x	0.00(2)	0.03(5)	-0.026(14)	0.029(15)
Goodness-of-fit on F^2, S	1.067	0.968	1.001	1.011
$R[I \geq 2\sigma(I)]/R$ [all data]	0.0282 / 0.0299	0.0509 /0.0537	0.0382 / 0.0577	0.0411 / 0.0654
$wR[I \geq 2\sigma(I)]/wR$ [all data]	0.0821 / 0.0852	0.1433 / 0.1485	0.0912 / 0.1055	0.0929 / 0.1060
Max. and min. el. dens. (e Å^{-3})	0.292 / -0.347	1.603 / -0.651	0.470 / -0.280	0.510 / -0.434

[a] Equal to independent reflections.

Magnetic measurements

Magnetic susceptibility was measured by Faraday method in fields up to 0.9 T in the temperature range from 2–300 K. At low temperatures susceptibility was measured in fields of

up to 0.2 T.

ESR experiments were performed on the polycrystalline forms as well as on the single crystals of the investigated compounds. For $[CuL^{A}(\mu\text{-Br})]_2$ only polycrystalline measurements were obtained due to small sizes of the single crystals. ESR experiments were carried out with a Bruker 580 FT/CW X-band spectrometer equipped with a standard Oxford Instruments model DTC2 temperature controller. The microwave frequency was $\approx$ 9.6 GHz with the magnetic field modulation amplitude of 0.5 mT at 100 kHz. Applied microwave power was 0.0002 mW and 0.2 mW for polycrystalline and single crystal measurements, respectively. The crystals of all compounds were elongated approximately along the crystallographic a-axis. They were rotated round three mutually orthogonal axes: a crystallographic a-axis and two chosen b'-axis and c'-axis. ESR spectra were recorded at 5° steps and the rotation was controlled by a home-made goniometer with the accuracy of 1°. A larger uncertainty (2–3°) was connected to the optimal deposition of the crystals on the quartz holder. The ESR spectra were measured from room down to liquid helium temperatures. At low temperatures (below ∼80 K) spectra were strongly influenced by the *passage effect* and therefore, these measurements were obtained carefully, by performing slow scans with small modulation amplitude at low microwave power and low modulation frequency.[36]

Results and Discussion

Description of structures

Reaction of ligands L^{A}=*N*-(L-alanine methyl ester)-*N'*-((2-pyridine-2-yl)methyl)oxalamide and L^{V}=*N*-(L-valine methyl ester)-*N'*-((2-pyridine-2-yl)methyl)oxalamide with $CuCl_2$ and $CuBr_2$ in MeOH results in crystals of the complexes $[CuL^{A}(\mu\text{-Cl})]_2$, $[CuL^{A}(\mu\text{-Br})]_2$ (which crystallized with two independent molecules in the asymmetric unit), $[CuL^{V}(\mu\text{-Cl})]_2$, and $[CuL^{V}(\mu\text{-Br})]_2$, that were analyzed by X-ray single crystal diffraction method (Fig. 1). The structures of these complexes are very similar with the structures of the dihalo-bridged Cu(II)

complexes we described previously.[13] Cu(II) ions are penta-coordinated by oxalamidato oxygen and nitrogen atoms, pyridyl nitrogen atom and two halogen ions (chlorides or bromides). The coordination polyhedron around the Cu(II) ion could be best described in these four complexes as an ideal or near ideal square pyramid, with $\tau = 0.00$–0.20 (Table 2), where $\tau = 0$ implies the ideal square-pyramidal geometry.[37] The square base coordination sites are occupied by a deprotonated ligand, thus acting as NNO tridentate ligand, and by one of the bridging halo-ions. The other bridging halo-ion occupies the apical position of the square pyramid (Fig. 1). The two Cu(II) centers are bridged by two halo-ions in such a way that two square pyramids share one base-to-apex edge with parallel basal planes. Such type of pyramidal arrangement in copper complexes containing the Cu–(μ–X)$_2$–Cu core is designated as a type II.[38]

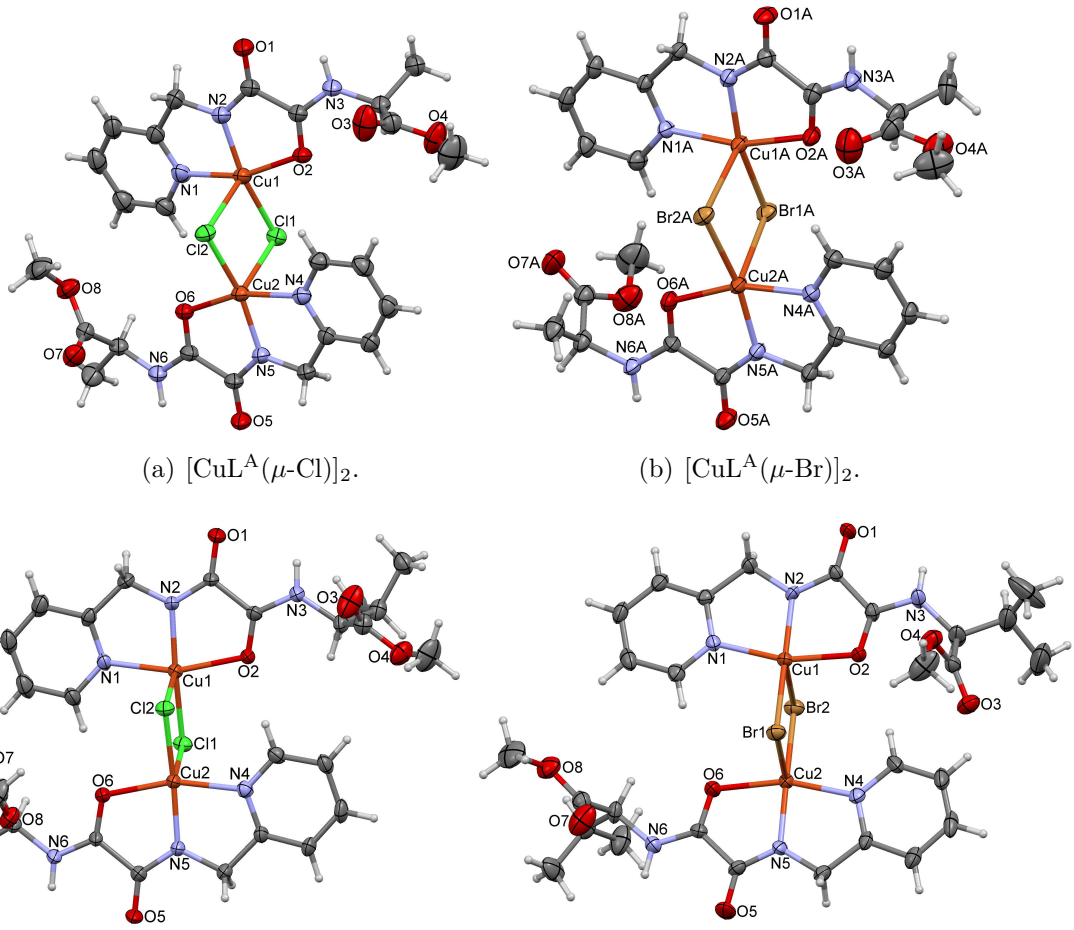

(a) $[CuL^{A}(\mu\text{-Cl})]_2$. (b) $[CuL^{A}(\mu\text{-Br})]_2$.

(c) $[CuL^{V}(\mu\text{-Cl})]_2$. (d) $[CuL^{V}(\mu\text{-Br})]_2$.

Figure 1: Molecular structures of $[CuL^{A}(\mu\text{-Cl})]_2$ (a), $[CuL^{A}(\mu\text{-Br})]_2$ (b), $[CuL^{V}(\mu\text{-Cl})]_2$(c), and $[CuL^{V}(\mu\text{-Br})]_2$ (d). Displacement ellipsoids for non-hydrogen atoms are drawn at the 30% probability level. Only one independent molecule (with only major component of disordered O3 atom) is presented for $[CuL^{A}(\mu\text{-Br})]_2$ (b).

Table 2: Molecular Geometry (Å; °; °Å^{-1}) of the Complexes Described in This Work

	$[CuL^A(\mu\text{-Cl})]_2$	$[CuL^V(\mu\text{-Cl})]_2$	$[CuL^A(\mu\text{-Br})]_2$[a]		$[CuL^V(\mu\text{-Br})]_2$
Cu–X[b] (basal)	2.2395(13)	2.2370(17)	2.3743(14)	2.3678(15)	2.3738(12)
	2.2424(12)	2.2373(16)	2.3800(15)	2.3646(15)	2.3787(12)
Cu–X (axial)(R)	2.7025(13)	2.7270(16)	2.8567(16)	2.9086(16)	2.8593(13)
	2.6885(12)	2.7280(17)	2.9399(17)	2.9893(16)	2.8779(14)
Cu–O (oxalamide)	2.064(3)	2.069(4)	2.066(6)	2.049(7)	2.037(6)
	2.044(3)	2.039(4)	2.042(7)	2.029(7)	2.044(6)
Cu–N (pyridyl)	2.019(4)	2.020(5)	2.032(7)	2.033(8)	2.036(7)
	2.027(4)	2.028(5)	2.025(8)	2.031(8)	2.005(7)
Cu–N (oxalamide)	1.908(4)	1.916(5)	1.911(8)	1.911(8)	1.894(7)
	1.910(3)	1.896(5)	1.923(8)	1.911(8)	1.914(7)
τ[c]	0.07	0.07	0.02	0.14	0.00
	0.01	0.04	0.07	0.20	0.04
d(Cu)[d]	0.2143(6)	0.1924(5)	0.1934(12)	0.1679(14)	0.1942(9)
	0.1843(6)	0.1676(5)	0.1796(14)	0.1340(14)	0.1860(9)
Cu$\cdots$Cu'	3.4253(8)	3.4574(6)	3.6457(19)	3.717(2)	3.5598(11)
Cu–X–Cu'(α)	87.57(4)	87.69(6)	85.93(5)	87.06(5)	84.77(4)
	87.17(4)	87.71(5)	87.75(5)	89.02(5)	85.10(4)
α/R	32.40	32.16	30.08	29.93	29.65
	32.42	32.15	29.85	29.78	29.57

[a] Data are given for two independent molecules.
[b] X = Cl or Br.
[c] Geometric parameter applicable to five-coordinate structures (degree of trigonality)[37] .
[d] Displacement of Cu(II) ions from the mean basal atoms plane.

The complexes are mutually linked by two N–H$\cdots$O hydrogen bonds between oxalamide moieties, so forming one-dimensional infinite chains of dinuclear units (Fig. 2 and Supporting Information (SI)). The hydrogen-bonded chains are further linked by other weak interactions into three-dimensional networks (for more detailed description of the structures see SI).

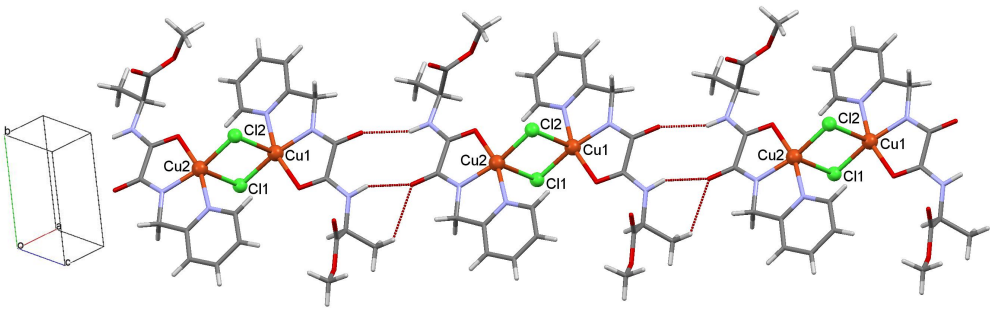

(a)

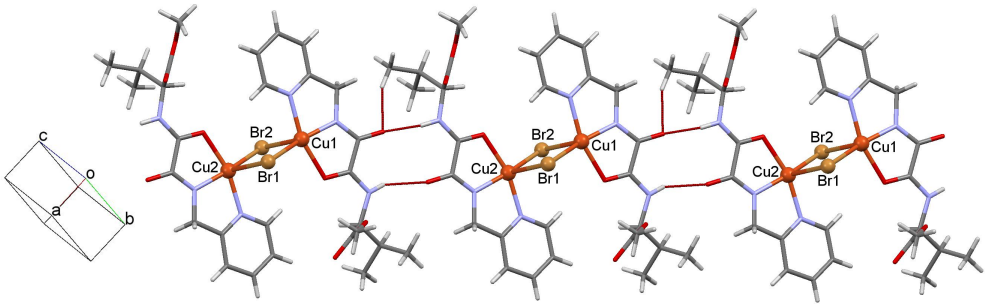

(b)

Figure 2: Capped stick representation of chain of dimers in $[CuL^{A}(\mu\text{-}Cl)]_2$ (a) and $[CuL^{V}(\mu\text{-}Br)]_2$ (b), showing N–H$\cdots$O and C–H$\cdots$O hydrogen bonds that form one-dimensional chains. Cu(II) ions and halogen ions are presented in ball and stick style. The chains formed in $[CuL^{A}(\mu\text{-}Br)]_2$ and $[CuL^{V}(\mu\text{-}Cl)]_2$ are presented in Figure S2 in SI.

Magnetic susceptibility

Temperature dependence of magnetic susceptibility of all the complexes is shown in Fig. 3. At low temperatures all complexes show deviation from Curie law (dashed line in all panels) signifying existence of weak antiferromagnetic interactions between spins.

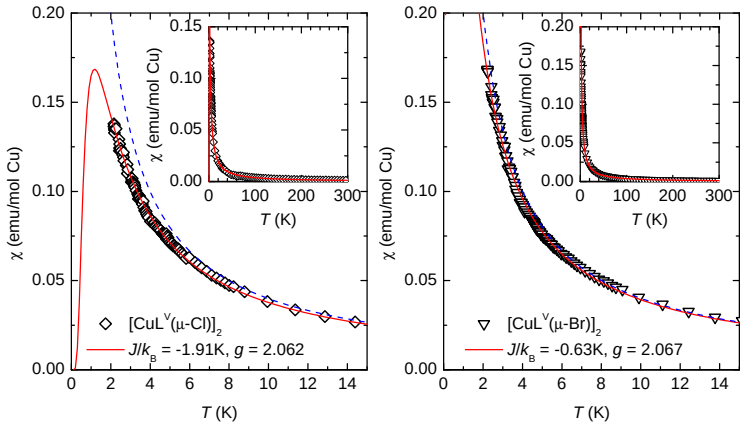

(a) $[\mathrm{CuL^V}(\mu\text{-Cl})]_2$ and $[\mathrm{CuL^V}(\mu\text{-Br})]_2$.

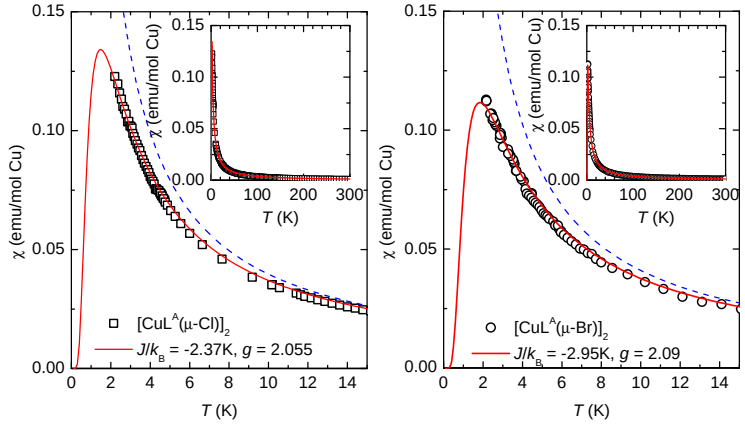

(b) $[\mathrm{CuL^A}(\mu\text{-Cl})]_2$ and $[\mathrm{CuL^A}(\mu\text{-Br})]_2$.

Figure 3: Temperature dependence of magnetic susceptibility of (a) valine complexes: $[\mathrm{CuL^V}(\mu\text{-Cl})]_2$ and $[\mathrm{CuL^V}(\mu\text{-Br})]_2$ and (b) alanine complexes: $[\mathrm{CuL^A}(\mu\text{-Cl})]_2$ and $[\mathrm{CuL^A}(\mu\text{-Br})]_2$. Solid lines represent fits to dimer model, and dashed line is Curie law for $S = 1/2$. Main panels show low-temperature range where susceptibility deviates from Curie law due to weak antiferromagnetic intradimer interactions. Insets show entire temperature range from $2 - 300$ K.

From crystal structures we expect weak magnetic dimers. In order to evaluate intradimer interaction J between the spins we fit the data to the isolated dimer model modified to include the influence of finite magnetic field on the singlet-triplet splitting at low temperatures.[39] Diamagnetic contribution for each complex was calculated using Pascal's constants[40] and appropriately taken into account. Obtained values of J are given in Table 3. All obtained values are antiferromagnetic and of the order of $1 - 2$ K.

Table 3: Intradimer Coupling J/k_B, g Factors and Pascal's Constants[40] Obtained by Fitting the Measured Data to the Dimer Model[39]

Compound	J/k_B (K)	g	Pascal's constant (emu/mol Cu)
$[\mathbf{CuL^A}(\mu\textbf{-Cl})]_2$	-2.37(1)	2.055	$-1.4355 \cdot 10^{-4}$
$[\mathbf{CuL^A}(\mu\textbf{-Br})]_2$	-2.95(1)	2.090	$-1.5475 \cdot 10^{-4}$
$[\mathbf{CuL^V}(\mu\textbf{-Cl})]_2$	-1.91(2)	2.062	$-1.6775 \cdot 10^{-4}$
$[\mathbf{CuL^V}(\mu\textbf{-Br})]_2$	-0.63(2)	2.067	$-1.7895 \cdot 10^{-4}$

ESR spectroscopy

Powder ESR spectra

The representative powder (polycrystalline) ESR spectra of the investigated compounds at three selected temperatures are shown in Fig. 4. Half-field ESR line at $g \sim 4$ connected with forbidden transition $\Delta M_S = \pm 2$ was not detected for any of the complexes.[1] The spectra can be simulated using only **g**-tensor parameters, while hyperfine **A**-tensors, due to interaction between electron and nuclear spin in copper ions, were not observed and therefore were neglected in further analysis. The spectra were simulated by *EasySpin* software[41] using Lorentzian lineshapes, allowing only linewidth to change with temperature. Values of **g**-tensors, obtained from simulation of the polycrystalline spectra, are shown in Table 4. Averaged values $\langle g \rangle$ are calculated as: $\langle g \rangle = \sqrt{(1/3)(g_x^2 + g_y^2 + g_z^2)}$.

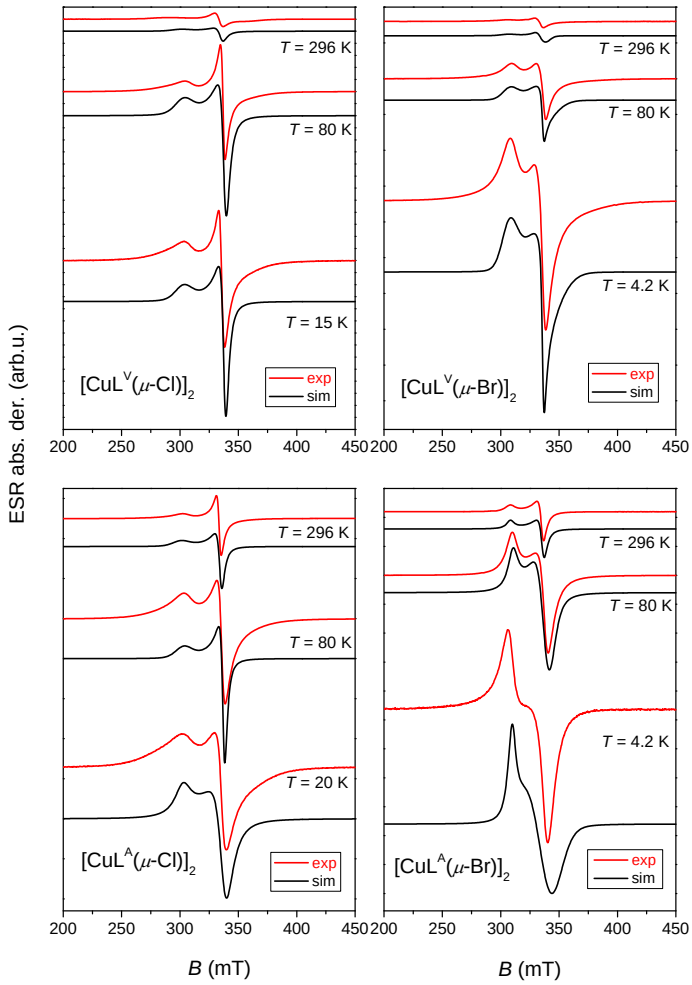

Figure 4: Experimental (red lines) and simulated (black lines) ESR spectra of polycrystalline samples of the compounds $[CuL^{V}(\mu\text{-Cl})]_2$, $[CuL^{V}(\mu\text{-Br})]_2$, $[CuL^{A}(\mu\text{-Cl})]_2$ and $[CuL^{A}(\mu\text{-Br})]_2$. The intensities of the spectra at different temperatures are presented in the real ratios, for each compound.

Table 4: Principal and Average Values of the Copper **g**-Tensors of the Investigated Compounds, Obtained From the Simulation of the Polycrystalline Spectra

Compound	g_x	g_y	g_z	$\langle g \rangle$
$\mathbf{[CuL^{A}(\mu\text{-Cl})]_2}$	2.055	2.055	2.290	2.136
$\mathbf{[CuL^{A}(\mu\text{-Br})]_2}$	2.050	2.050	2.235	2.113
$\mathbf{[CuL^{V}(\mu\text{-Cl})]_2}$	2.050	2.050	2.290	2.133
$\mathbf{[CuL^{V}(\mu\text{-Br})]_2}$	2.030	2.067	2.254	2.119

As can be seen from Fig. 4, the simulations reproduce well the experimentally observed spectra for all compounds. The obtained axial **g**-tensor parameters for $[CuL^{V}(\mu\text{-Cl})]_2$, $[CuL^{A}(\mu\text{-Cl})]_2$ and $[CuL^{A}(\mu\text{-Br})]_2$ with $g_z > g_y = g_x$ reveal that the ground state of unpaired electron is the $d_{x^2-y^2}$ orbital. For $[CuL^{V}(\mu\text{-Br})]_2$ the "rhombic" spectra are obtained with $g_z > g_y > g_x$ and a ratio $(g_y - g_x)/(g_z - g_y) = 0.198 < 1$ shows that the ground state is predominantly also $d_{x^2-y^2}$.[42,43] The obtained results are in agreement with the square-pyramidal coordinations around copper ions and $d_{x^2-y^2}$ orbital with unpaired electron is localized in the basal plane of square pyramid.

Lorentzian line shapes and the absence of hyperfine structures point to the presence of the exchange interaction while the spectral simulations reveal that exchange interactions in these compounds are weak, in agreement with the susceptibility measurement results.

Single crystal spectra

Due to small sizes of $[CuL^{A}(\mu\text{-Br})]_2$ crystals, its single crystal ESR spectra was not recorded while the spectra of the other three compounds show very complex structures. The complexes $[CuL^{A}(\mu\text{-Cl})]_2$ and $[CuL^{V}(\mu\text{-Br})]_2$ have a single line in one rotation plane while in other two planes single or double lines occurred depending on the position of the crystals in the magnetic field. The complex $[CuL^{V}(\mu\text{-Cl})]_2$ shows one or two lines in all three rotation planes. The shape of all lines were Lorentzian-like. The complete angular dependence of the single crystal spectra of $[CuL^{V}(\mu\text{-Cl})]_2$ at room temperatures is presented in Fig. 5, while the spectra of $[CuL^{V}(\mu\text{-Br})]_2$ and $[CuL^{A}(\mu\text{-Cl})]_2$ are given in Figures S6 and S8 in SI.

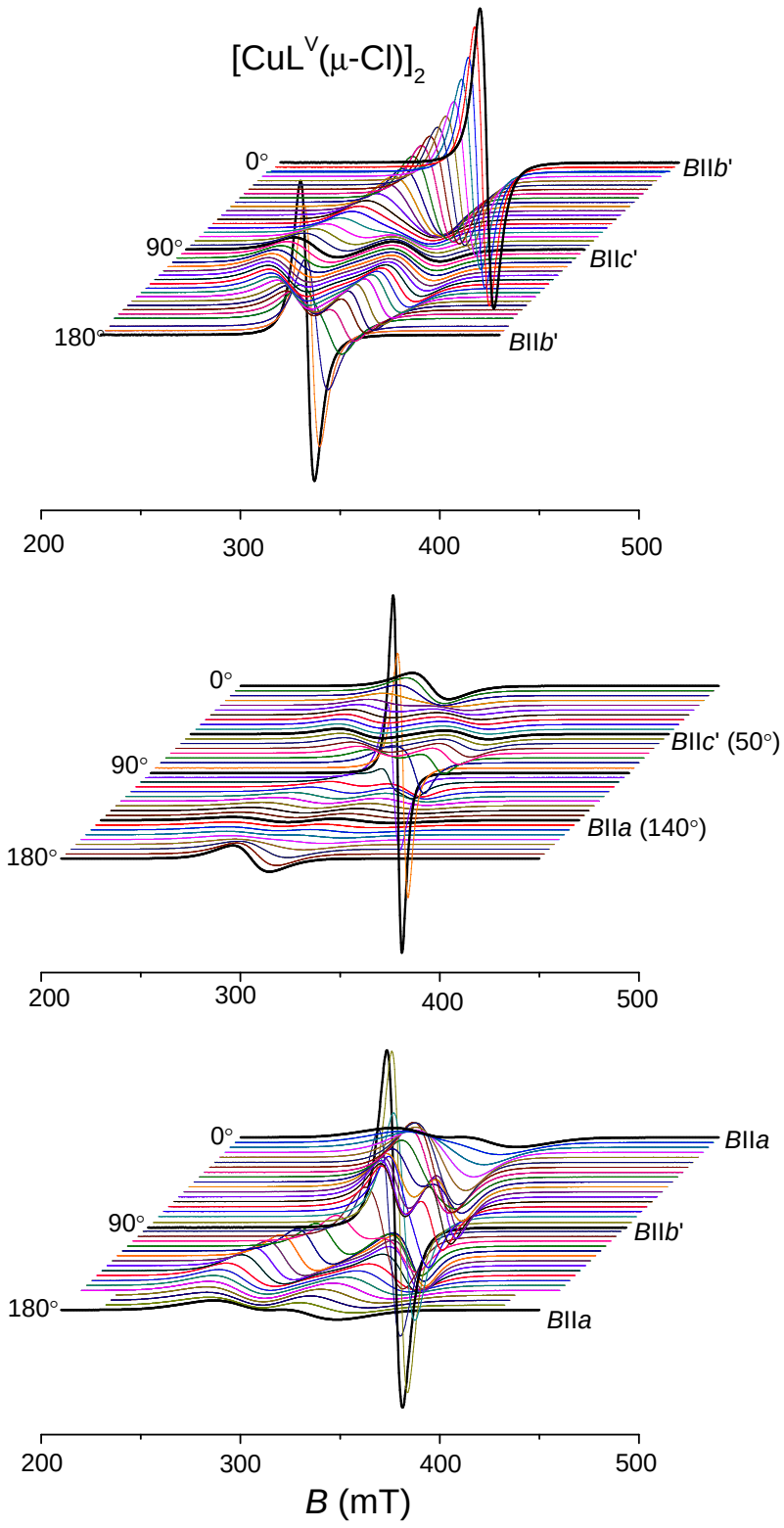

Figure 5: Angular variation of the single crystal ESR spectra of compound $[CuL^{V}(\mu\text{-}Cl)]_2$, in three mutually perpendicular planes, at room temperature.

The corresponding angular dependence of the effective g_{eff}-values and peak-to-peak linewidths W_{pp} for all three rotation planes for $[CuL^{V}(\mu\text{-Cl})]_2$ complex is shown in Fig. 6 while the dependencies for $[CuL^{V}(\mu\text{-Br})]_2$ and $[CuL^{A}(\mu\text{-Cl})]_2$ are given in Figures S7 and S9 in SI. Here g_{eff} presents g-value at resonance field, defined as $h\nu = g_{eff}\mu_B H_{res}$, where ν is the applied microwave frequency, h is Planck constant and μ_B Bohr magneton. g_{eff} and W_{pp}-values are obtained using Bruker Elexsys Xepr software. The values of g_{eff} and W_{pp} at $T = 80$ K were approximately the same as those at room temperature and therefore, they are omitted. At lower temperatures the angular dependencies were not recorded due to strong *passage effect*[36] that caused distortion of spectra.

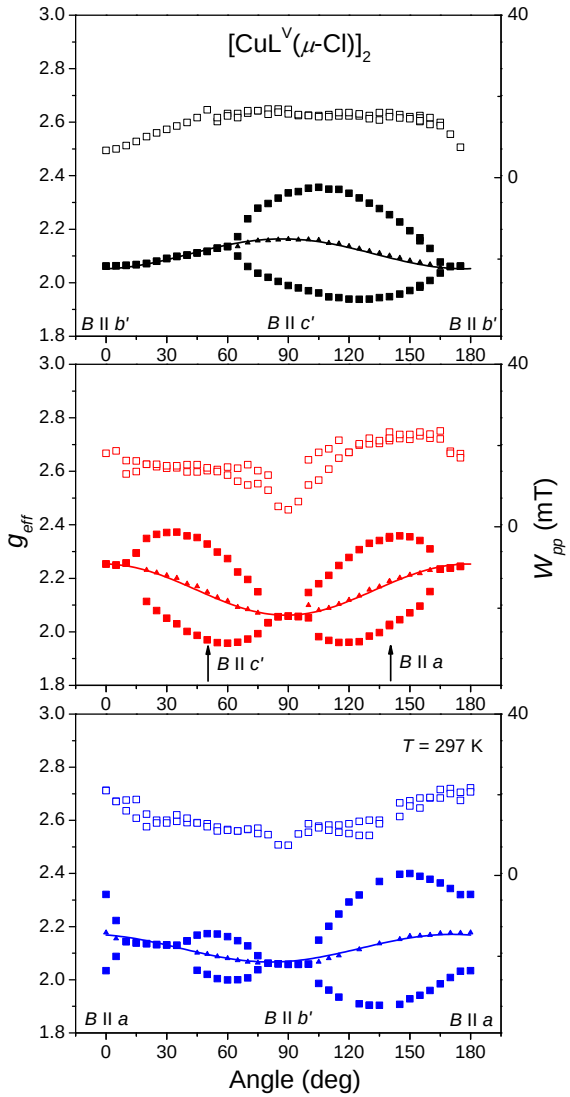

Figure 6: Angular variation of the g_{eff}-values (solid squares) and the W_{pp} linewidths (open squares) of ESR lines for the single crystal of $[CuL^{V}(\mu\text{-}Cl)]_2$, at room temperature, for three mutually perpendicular planes. Solid triangles represent the average g_{av}-values calculated as $g_{av} = (g_1 + g_2)/2$.

The observed number of resonance lines can not be simply correlated to the number of molecules (dimers), Z, found in the unit cell. Namely, for $[CuL^{V}(\mu\text{-}Cl)]_2$ and $[CuL^{V}(\mu\text{-}Br)]_2$ $Z = 1$, while $Z = 2$ for $[CuL^{A}(\mu\text{-}Cl)]_2$ complex (Table 1). Two bridged coppers in dimers are crystallographically nonequivalent but these differences are small, as can be seen from Table 2, and they can not produce observed ESR line splitting. Namely, observed resonance lines are not described by physical copper g-values but rather with previously mentioned

effective values that range from $g_{eff} \approx 1.9$ to $g_{eff} \approx 2.4$. Furthermore, following Ref. 12 if we use the average g_{av}-values, calculated as $g_{av} = (g_1 + g_2)/2$ (presented as solid triangles in Fig. 6) and perform fit to well-known expression:

$$\begin{aligned} g^2 = \quad & (\mathbf{g^T g})_{aa} \sin^2\theta \cos^2\phi + (\mathbf{g^T g})_{ab'} \sin^2\theta \sin 2\phi + \\ & + (\mathbf{g^T g})_{b'b'} \sin^2\theta \sin^2\phi + (\mathbf{g^T g})_{ac'} \sin 2\theta \cos\phi + \\ & + (\mathbf{g^T g})_{b'c'} \sin 2\theta \sin\phi + (\mathbf{g^T g})_{c'c'} \cos^2\theta \end{aligned} \tag{1}$$

it is possible to obtain the corresponding principal values of molecular **g**-tensor. Here θ and ϕ are the polar and azimuthal angles of the magnetic field vector **B**, respectively and (a, b', c') is our laboratory coordinate system.[44] Results of fitting data to Eq. 1 are shown as solid lines in Fig. 6. However, these eigenvalues, given in Table S3, are in disagreement with the values given in Table 4 and can not simulate satisfactorily polycrystalline spectra, for all three investigated compounds. Therefore, two resonance lines observed in spectra could not been assigned to g-factors of two nonequivalent copper ions in dimers but rather to two energy transitions due to coupling between coppers, as will be shown in the next section.

Intradimer interactions

Generally, two copper(II) centers in dimers can be described by the effective spin-Hamiltonian:[1,3,12]

$$\mathbf{H} = \mu_B(\mathbf{S_1} \cdot \mathbf{g_1} + \mathbf{S_2} \cdot \mathbf{g_2}) \cdot \mathbf{B} + \mathbf{S_1} \cdot (-J\mathbf{I} + \mathbf{D}) \cdot \mathbf{S_2}. \tag{2}$$

In Eq. 2, **S** and **g** are the spin operators and **g**-tensors, respectively, for two nonequivalent copper ions Cu1 and Cu2 in dimer, **B** is the magnetic field, J is the isotropic exchange interaction constant between Cu1 and Cu2, **I** is the unit matrix and **D** is the second rank symmetric tensor that describes both dipole-dipole and symmetric anisotropic exchange interactions.[3,12] In all complexes inversion center between two copper ions in dimer is missing which allows for presence of antisymmetric anisotropic Dzyaloshinskii-Moriya interaction

in Hamiltonian. To simplify our analysis, we omit this contribution and leave the study of antisymmetric anisotropic exchange in title compounds for the future. Anisotropic exchange contribution due to spin-orbit coupling is also usually negligible compared to the intradimer dipolar contribution.[16] Hyperfine interaction was not experimentally observed, as it is previously mentioned, and therefore its term is omitted in Eq. 2. From the similar local coordinations around nonequivalent copper ions in dimers, as can be seen from Table 2, identical g-values for coppers can be used.

In a first-order approximation for two identical spins with isotropic g-values, taking only the secular term of the dipolar interaction and D parameter sufficiently small compared to the Zeeman energy, Eq. 2 predicts two ESR lines separated by the value ΔH, expressed in the magnetic field units:[12,45]

$$\Delta H = a\frac{3}{2}\frac{g\mu_B}{r^3}(1 - 3cos^2\varphi), \tag{3}$$

where $\mathbf{r}$ is the distance between spins, φ is the angle between $\mathbf{r}$ and $\mathbf{B}$ and a is a factor of proportionality. In fitting our data to Eq. 3, we took into account the fact that vector $\mathbf{r}$ is not in the plane of crystal rotation in magnetic field and corrected the formula 3 accordingly. For *pure* dipolar behavior, parameter a should be equal to 1. In Fig. 7 we compare experimentally obtained difference of the resonance fields of two observed lines $\Delta H_{res} = (h\nu/\mu_B)(1/g_1 - 1/g_2)$, with the difference ΔH predicted by Eq. 3 for the compound $[\mathrm{CuL^V}(\mu\text{-Cl})]_2$.

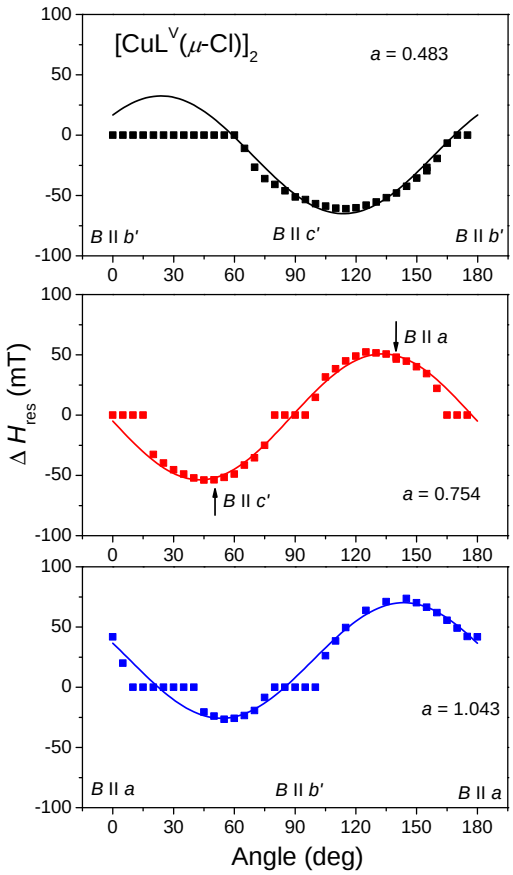

Figure 7: Angular variation of the difference of the resonance field of two observed lines ΔH_{res} obtained experimentally (solid symbols) and simulated according to Eq. 3 (solid lines) for the single crystal of $[CuL^{V}(\mu\text{-Cl})]_2$, at room temperature, for three mutually perpendicular planes. The parameter a obtained from the simulation is indicated in the figure.

From Fig. 7 one can conclude that the main cause of the observed line splitting is intradimer dipole-dipole interaction. The corresponding comparison for $[CuL^{V}(\mu\text{-Br})]_2$ and $[CuL^{A}(\mu\text{-Cl})]_2$ complexes is omitted because of experimentally observed mostly collapsed lines.

If we estimate dipolar contribution as $D^{dip}(\text{cm}^{-1}) \approx 0.433 g_z^2/r^3$, where r is the Cu–Cu separation in Å[1,16] the value of 50 mT$\approx$ 0.08 K is obtained, for $[CuL^{V}(\mu\text{-Cl})]_2$. For $[CuL^{V}(\mu\text{-Br})]_2$ and $[CuL^{A}(\mu\text{-Cl})]_2$ complexes, the corresponding values are 0.07 and 0.08 K, respectively. These values are quite large, few percents of exchange coupling constant J. For comparison, hyperfine contribution is usually $A_{\|} \approx 20$ mT for copper[46,47] and that is why

this interaction is not observed in experiments. Observed collapsing or merging of split lines, as well as the obtained value of parameter $a < 1$ for two rotation planes, point to the presence of weak interdimer exchange interaction described by parameter J'.[12]

Interdimer exchange interaction

Observed split resonance lines, instead of simple crossing at the *magic angles* where $\Delta H_{res} = 0$, show sudden merging and they stay merged in the broad angular ranges.[19] Collapsing of ESR line is described by a phenomena of exchange narrowing, due to interdimer interactions.[7,12,14–25] Here, the peak-to-peak linewidth of the observed resonance lines is relatively constant, except in the *merging regions* where significant narrowing, accompanied by corresponding high spectral intensity, is present, as can be seen in Fig. 5, as well as in Figures S6 and S8 in SI. For weak exchange interaction $J' < D$, two split lines are shifted to the center of the spectra (parameter $a < 1$) and broadened while for strong exchange $J' > D$, the two lines merge into one.[7,12] Here presented spectra show partially resolved ESR lines and therefore, one can roughly estimate interdimer exchange interaction as $J' \approx D$. Using only dipolar contribution to D, the value of $J' \approx 0.07 - 0.08$ K can be approximated.

Better estimation is obtained applying Anderson's stochastic theory, where the transition from weak to strong exchange regime was analyzed using the so-called random frequency modulation model[20,21] that has been exploited in a number of cases.[7,12,18,19,23] The second approach is a quantum perturbative model introduced by Kubo and Tomita.[14] Here we used third, simplest model presented by Hoffmann and coworkers.[15–17,26,27] All three approaches have been applied to the same system and gave similar results.[23] Using generalized Bloch equations for spins jumping between two paramagnetic centers that are exchange coupled via parameter J', Hoffmann and coworkers derived an expression for an intensity of single crystal spectrum composed of two Lorentzian lines with half-widths Γ_1 and Γ_2 at resonance

fields B_1 and B_2:[17,27]

$$Y(B) = N(W_1^2 + W_2^2)^{-2}\{[W_2 - 2(B - B_0)J'](W_1^2 + W_2^2)$$
$$- 4[(B - B_0)W_2 - (\Gamma_0 + 2J')W_1] \cdot [(B - B_0)W_1 + (\Gamma_0 + J')W_2]\},$$

where

$$W_1 = (B - B_1)(B - B_2) - (\Gamma_1 + K_1)(\Gamma_2 + K_2) + K_1K_2,$$
$$W_2 = (B - B_1)(\Gamma_2 + K_2) + (B - B_2)(\Gamma_1 + K_1),$$
$$\Gamma_0 = (\Gamma_1 + \Gamma_2)/2, B_0 = (B_1 + B_2)/2,$$
$$K_1 = J'B_1/B_0, K_2 = J'B_2/B_0. \quad (4)$$

Here, N is a normalization factor connected with a number of spins and all parameters are given in magnetic field units. When $J' = 0$, Eq. 4 describes the spectrum of two Lorentzian lines placed at field B_1 and B_2, while when J' increases, the merging effect appears. The fitting of Eq. 4 to experimentally observed spectra was performed and few representative spectra are shown in Fig. 8.

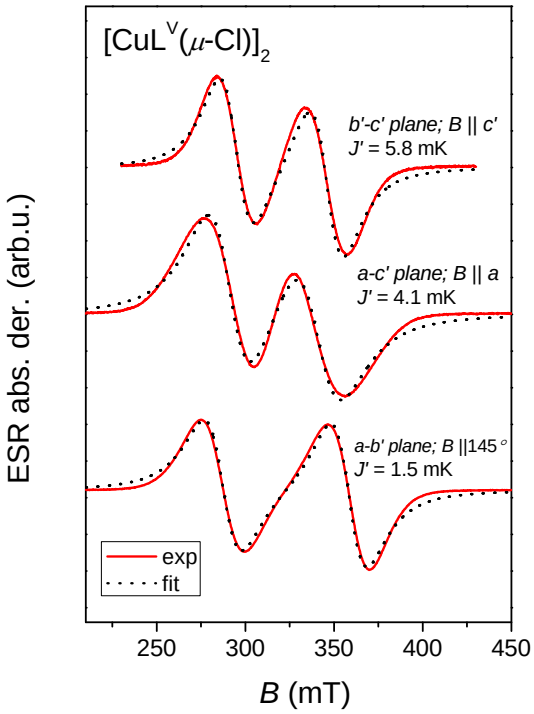

Figure 8: The representative ESR spectra for the single crystal of $[CuL^{V}(\mu\text{-}Cl)]_2$ in three rotation planes at room temperature. Dotted lines represent the best fitting of Eq. 4 to experimental spectra, with indicated J' values, obtained from the fitting. Intensities of the lines are scaled to have same heights.

We see that an agreement between fitted and experimentally obtained spectra is very well. Generally, the fitting is better when two lines are more separated compared to situation when one merged line is observed. The values of interdimer exchange parameters obtained from the fitting are $J' \sim 1.5 - 5.8$ mK, one order of magnitude smaller compared to previously roughly estimated values.

Conclusion

Set of four dihalo-bridged copper(II) dimers were synthesized and thoroughly characterized. Single-crystal X-ray diffraction analysis revealed that, in all cases, the Cu(II) ion is penta-

coordinated by a tridentate NNO ligand and by two halo-ions (Cl or Br) in an ideal or near ideal square-pyramidal environment, in such a way that two pyramids share one base-to-apex edge with parallel basal planes. The main hydrogen-bonded motif in these complexes is one-dimensional infinite chain primarily formed by N–H$\cdots$O hydrogen bonds. Magnetization measurements discovered the presence of weak antiferromagnetic interactions between the copper ions in dimers, ($|J| \approx 0.6-3$ K), in agreement with the small values found for similar dihalo-bridged copper compounds.[13,38,48–51] This relatively weak exchange interaction was confirmed by powder ESR experiments, that showed that unpaired copper electrons are localized in $d_{x^2-y^2}$ orbitals, placed in almost parallel basal planes of bipyramids.

However, the central observation in this work is the detection of unusual anisotropic splitting and merging of ESR lines when single crystals rotate in magnetic field. This splitting was assigned to intradimer dipole-dipole interaction while partial merging of lines revealed existence of weak interdimer exchange interaction, mediated via hydrogen bonded polynuclear arrangements. Using theoretical model introduced by Hoffmann and coworkers[15–17,26,27] weak interdimer exchange interaction parameter was estimated to be of the order of $|J'| \sim 1$ mK.

Despite very similar structures of complexes described here compared with the complexes previously reported,[13] described by similar X-ray, magnetization and powder ESR results, we probed small but significant difference in magnetic properties using single crystal ESR spectroscopy. Therefore, single-crystal ESR spectroscopy has proven to be adequate technique to detect small differences in weak magnetic interactions due to slightly different local environment of magnetic centers, usually non-visible by standard characterization techniques.

Supporting Information Available

The following files are available free of charge.

- Additional crystallographic details for structures described in the paper

- g-values from averaged single crystal resonance lines
- Angular variation of the single crystal ESR spectra of $[CuL^{V}(\mu\text{-}Br)]_2$ and $[CuL^{A}(\mu\text{-}Cl)]_2$
- Angular variation of g_{eff}-values and the W_{pp} linewidths of $[CuL^{V}(\mu\text{-}Br)]_2$ and $[CuL^{A}(\mu\text{-}Cl)]_2$
- CCDC 1521402-1521405
- CIF files

Acknowledgement

This work was fully supported by the Croatian Science Foundation under grant HrZZ UIP-2014-09-9775. D. M. and Z. Dž. thank the European Union Seventh Framework Programme (FP7 2007-2013) under grant agreement n° 291823 Marie Curie FP7-PEOPLE-2011-COFUND (The new International Fellowship Mobility Programme for Experienced Researchers in Croatia - NEWFELPRO).

References

(1) Bencini, A.; Gatteschi, D. *Electron Paramagnetic Resonance of Exchange Coupled Systems*; Springer-Verlag: Berlin Heidelberg, 1990.

(2) Gatteschi, D.; Sessoli, R.; Villain, J. *Molecular Nanomagnets*; Oxford University Press: Oxford, UK, 2006.

(3) Kahn, O. *Molecular Magnetism*; Wiley-VCH Inc., 1993.

(4) Upadhyay, A. K.; Petasis, D. T.; Arciero, D. M.; Hooper, A. B.; Hendrich, M. P. Spectroscopic Characterization and Assignment of Reduction Potentials in the Tetra-

heme Cytochrome c_{554} from *Nitrosomonas Europaea*. *J. Am. Chem. Soc.* **2003**, *125*, 1738–1747.

(5) Astashkin, A. V.; Elmore, B. O.; Fan, W.; Guillemette, J. G.; Feng, C. Pulsed EPR Determination of the Distance Between Heme Iron and FMN Centers in a Human Inducible Nitric Oxide Synthase. *J. Am. Chem. Soc.* **2010**, *132*, 12059–12067.

(6) Gómez, M. C.; Neuman, N. I.; Dalosto, S. D.; González, P. J.; Moura, J. J. G.; Rizzi, A. C.; Brondino, C. D. Isotropic Exchange Interaction Between Mo and the Proximal FeS Center in the Xanthine Oxidase Family Member Aldehyde Oxidoreductase from Desulfovibrio Gigas on Native and Polyalcohol Inhibited Samples: an EPR and QM/MM Study. *J. Biol. Inorg. Chem.* **2015**, *20*, 233–242.

(7) Neuman, N. I.; Burna, E.; Baggio, R.; Passeggi, M. C. G.; Rizzi, A. C.; Brondino, C. D. Transition from Isolated to Interacting Copper(II) Pairs in Extended Lattices Evaluated by Single Crystal EPR Spectroscopy. *Inorg. Chem. Front.* **2015**, *2*, 837–845.

(8) Rodríguez-Fortea, A.; Alemany, P.; Alvarez, S.; Ruiz, E. Exchange Coupling in Halo-Bridged Dinuclear Cu(II) Compounds: A Density Functional Study. *Inorg. Chem.* **2002**, *41*, 3769–3778.

(9) Gungor, E.; Kara, H. Chiral One-Dimensional Hydrogen Bonded, Antiferromagnetic Chloro-Bridged Dinuclear Copper(II) Complex with Tridentate Schiff Base Ligand. *Inorg. Chim. Acta* **2012**, *384*, 137–142.

(10) Rojo, T.; Arriortua, M. I.; Ruiz, J.; Darriet, J.; Villeneuve, G.; Beltran-Porter, D. Magnetostructural Correlations in Parallel Square-Planar Chloride Bridged Copper(II) Dimers: Structure, Dynamic Nuclear Magnetic Resonance Study, and Magnetic Properties of $[Cu_2(terpy)_2Cl_2][PF_6]_2$. *J. Chem. Soc., Dalton Trans.* **1987**, 285–291.

(11) Landee, C. P.; Greeney, R. E. Strong Antiferromagnetic Exchange in a Bromide-Bridged Copper Dimer, bis(μ-bromo)bis[bromobis(tetramethylene sulfoxide)copper(II)]. Struc-

ture, Susceptibility, and Magnetostructural Correlations. *Inorg. Chem.* **1986**, *25*, 3771–3775.

(12) Neuman, N. I.; Perec, M.; González, P. J.; Passeggi, M. C. G.; Rizzi, A. C.; Brondino, C. D. Single Crystal EPR Study of the Dinuclear Cu(II) Complex [Cu(tda)(phen)]2·H_2tda (tda = Thiodiacetate, phen = Phenanthroline): Influence of Weak Interdimeric Magnetic Interactions. *J. Phys. Chem. A* **2010**, *114*, 13069–13075.

(13) Žilić, D.; Rakvin, B.; Milić, D.; Pajić, D.; Đilović, I.; Cametti, M.; Džolić, Z. Crystal Structures and Magnetic Properties of a Set of Dihalo-Bridged Oxalamidato Copper(II) Dimers. *Dalton Trans.* **2014**, *43*, 11877–11887.

(14) Kubo, R.; Tomita, K. A General Theory of Magnetic Resonance Absorption. *J. Phys. Soc. Jap.* **1954**, *9*, 888–919.

(15) Hoffmann, S. Temperature Dependence of a Superexchange Interaction Determined from Merging Effect of Copper(II) EPR Lines. *Chem. Phys. Lett.* **1983**, *98*, 329–332.

(16) Hoffmann, S. K.; Towle, D. K.; Hatfield, W. E.; Chaudhuri, P.; Wieghardt, K. Study of Intradimer and Interdimer Exchange Interactions in Dichloro-bis(diethylenetriamine)dicopper Perchlorate ($[Cu_2(dien)_2Cl_2](ClO_4)_2$) by Electron Paramagnetic Resonance and Magnetic Susceptibility Measurements. *Inorg. Chem.* **1985**, *24*, 1307–1312.

(17) Hoffmann, S. K.; Hilczer, W.; Goslar, J. Weak long-distance Superexchange Interaction and its Temperature Variations in Copper(II) Compounds Studied by Single Crystal EPR. *Appl. Magn. Reson.* **1994**, *7*, 289–321.

(18) Brondino, C. D.; Calvo, R.; Atria, A. M.; Spodine, E.; Nascimento, O. R.; Peña, O. Magnetic Interactions in the Copper Complex (l-Aspartato)(1,10-phenanthroline)copper(II) Hydrate. An Exchange-Coupled Extended System with Two Dissimilar Copper Ions. *Inorg. Chem.* **1997**, *36*, 3183–3189.

(19) Calvo, R.; Abud, J. E.; Sartoris, R. P.; Santana, R. C. Collapse of the EPR Fine Structure of a One-Dimensional Array of Weakly Interacting Binuclear Units: A Dimensional Quantum Phase Transition. *Phys. Rev. B* **2011**, *84*, 104433–1–104433–13.

(20) Anderson, P. W.; Weiss, P. R. Exchange Narrowing in Paramagnetic Resonance. *Rev. Mod. Phys.* **1953**, *25*, 269–276.

(21) Anderson, P. W. A Mathematical Model for the Narrowing of Spectral Lines by Exchange or Motion. *J. Phys. Soc. Jap.* **1954**, *9*, 316–339.

(22) Hoffmann, S. K.; Goslar, J.; Hilczer, W.; Goher, M. A.; Luo, B.-S.; Mak, T. C. Crystal Structure, Dynamic and Dipolar Effects in EPR Spectra of Cu(2-benzoylpyridine)$_2$(ClO_4)$_2$ [Cu($C_{12}H_9NO$)$_2$(ClO_4)$_2$] Crystals with Negligible Exchange Interaction. *J. Phys. Chem. Solids* **1997**, *58*, 1351–1358.

(23) Calvo, R. EPR Measurements of Weak Exchange Interactions Coupling Unpaired Spins in Model Compounds. *Appl. Magn. Reson.* **2007**, *31*, 271–299.

(24) Napolitano, L. M. B.; Nascimento, O. R.; Cabaleiro, S.; Castro, J.; Calvo, R. Isotropic and Anisotropic Spin-Spin Interactions and a Quantum Phase Transition in a Dinuclear Cu(II) Compound. *Phys. Rev. B* **2008**, *77*, 214423–1–214423–13.

(25) Neuman, N. I.; Franco, V. G.; Ferroni, F. M.; Baggio, R.; Passeggi, M. C. G.; Rizzi, A. C.; Brondino, C. D. Single Crystal EPR of the Mixed-Ligand Complex of Copper(II) with l-Glutamic Acid and 1,10-Phenanthroline: A Study on the Narrowing of the Hyperfine Structure by Exchange. *J. Phys.Chem. A* **2012**, *116*, 12314–12320.

(26) Hoffmann, S. K.; Goslar, J.; Szczepaniak, L. S. Weak Exchange Interaction in cis-Cu(NH_2CH_2COO)$_2$·H_2) Single Crystal: EPR Studies. *Phys. Rev. B* **1988**, *37*, 7331–7336.

(27) Hilczer, W.; Goslar, J.; Tritt-Goc, J.; Hoffmann, S. K. Weak Inter- and Intralayer Exchange Coupling between Copper(II) Dimers and a Triplet Density Effect in EPR of Tris(ethylenediamine)cobalt(III) Bis(μ-chloro)bis[trichlorocuprate(II)] Dichloride Dihydrate. *Inorg. Chem.* **1995**, *34*, 1852–1858.

(28) Džolić, Z.; Cametti, M.; Milić, D.; Žinić, M. The Formation of $CuCl_2$-Specific Metallogels of Pyridyloxalamide Derivatives in Alcohols. *Chem.-Eur. J.* **2013**, *19*, 5411–5416.

(29) *CrysAlis PRO*; Agilent Technologies Ltd., Yarnton, Oxfordshire: England, 2014.

(30) Sheldrick, G. M. Crystal Structure Refinement with *SHELXL*. *Acta Crystallogr.* **2015**, *C71*, 3–8.

(31) Burla, M. C.; Caliandro, R.; Camalli, M.; Carrozzini, B.; Cascarano, G. L.; De Caro, L.; Giacovazzo, C.; Polidori, G.; Spagna, R. *SIR2004*: an Improved Tool for Crystal Structure Determination and Refinement. *J. Appl. Crystallogr.* **2005**, *38*, 381–388.

(32) Farrugia, L. J. *WinGX* and *ORTEP for Windows*: an Update. *J. Appl. Crystallogr.* **2012**, *45*, 849–854.

(33) Spek, A. L. Structure Validation in Chemical Crystallography. *Acta Crystallogr.* **2009**, *D65*, 148–155.

(34) Spek, A. L. *PLATON* SQUEEZE: a Tool for the Calculation of the Disordered Solvent Contribution to the Calculated Structure Factors. *Acta Crystallogr.* **2015**, *C71*, 9–18.

(35) Macrae, C. F.; Bruno, I. J.; Chisholm, J. A.; Edgington, P. R.; McCabe, P.; Pidcock, E.; Rodriguez-Monge, L.; Taylor, R.; Van De Streek, J.; Wood, P. A. Mercury CSD 2.0 - New Features for the Visualization and Investigation of Crystal Structures. *J. Appl. Crystallogr.* **2008**, *41*, 466–470.

(36) Eaton, G.; Eaton, S.; Barr, D.; Weber, R. *Quantitative EPR*; Springer Vienna, 2010.

(37) Addison, A. W.; Rao, T. N.; Reedijk, J.; van Rijn, J.; Verschoor, G. C. Synthesis, Structure, and Spectroscopic Properties of Copper(II) Compounds Containing Nitrogen-Sulphur Donor Ligands; the Crystal and Molecular Structure of aqua[1,7-bis(N-methylbenzimidazol-2[prime or minute]-yl)-2,6-dithiaheptane]copper(II) perchlorate. *J. Chem. Soc., Dalton Trans.* **1984**, 1349–1356.

(38) Rodríguez, M.; Llobet, A.; Corbella, M.; Martell, A. E.; Reibenspies, J. Synthesis, Structure, and Magnetic Properties of a New Chloro-Bridged Dimer $[Cu_2(dpt)_2Cl_2]Cl_2$ with an Unusual Structure and Ferromagnetic Coupling. *Inorg. Chem.* **1999**, *38*, 2328–2334.

(39) Myers, B. E.; Berger, L.; Friedberg, S. A. Low-Temperature Magnetization of $Cu(NO_3)_2 \cdot 2.5H_2O$. *J. of Appl. Phys.* **1969**, *40*, 1149–1151.

(40) Bain, G. A.; Berry, J. F. Diamagnetic Corrections and Pascal's Constants. *J. Chem. Educ.* **2008**, *85*, 532–536.

(41) Stoll, S.; Schweiger, A. EasySpin, a Comprehensive Software Package for Spectral Simulation and Analysis in EPR. *J Magn Reson.* **2006**, *178*, 42–55.

(42) Garribba, E.; Micera, G. The Determination of the Geometry of Cu(II) Complexes: An EPR Spectroscopy Experiment. *J. Chem. Educ.* **2006**, *83*, 1229–1232.

(43) Jurić, M.; Molčanov, K.; Žilić, D.; Kojić-Prodić, B. From Mononuclear to Linear One-Dimensional Coordination Species of Copper(II)-Chloranilate: Design and Characterization. *RSC Adv.* **2016**, *6*, 62785–62796.

(44) Weil, J. A.; Bolton, J. R.; Wertz, J. E. *Electron Paramagnetic Resonance*; John Wiley and Sons, Inc.: New York, 1994.

(45) Carrington, A.; D., M. A. *Introduction to Magnetic Resonance*; Harper and Row: New York, 1967.

(46) Jurić, M.; Pajić, D.; Žilić, D.; Rakvin, B.; Molčanov, K.; Popović, J. Magnetic Order in a Novel 3D Oxalate-Based Coordination Polymer $[Cu(bpy)_3][Mn_2(C_2O_4)_3]\cdot H_2O_n$. *Dalton Trans.* **2015**, *44*, 20626–20635.

(47) Androš, L.; Jurić, M.; Planinić, P.; Žilić, D.; Rakvin, B.; Molčanov, K. New Mononuclear Oxalate Complexes of Copper(II) with 2D and 3D Architectures: Synthesis, Crystal Structures and Spectroscopic Characterization. *Polyhedron* **2010**, *29*, 1291 – 1298.

(48) Singh, P.; Jeter, D. Y.; Hatfield, W. E.; Hodgson, D. J. Out-of-Plane Interactions in Parallel-Planar Copper(II) Dimers. Structure and Magnetic Properties of dibromobis(2-methylpyridine)copper(II). *Inorg. Chem.* **1972**, *11*, 1657–1661.

(49) Phelps, D. W.; Goodman, W. H.; Hodgson, D. J. Structural Characterization of bis[dibromo(N,N-dimethylethylenediamine)copper(II)] and bis[dichloro(N,N-dimethylethylenediamine)copper(II)], $[Cu(dmen)Br_2]_2$ and $[Cu(dmen)Cl_2]_2$. *Inorg. Chem.* **1976**, *15*, 2266–2270.

(50) Rojo, T.; Arriortua, M. I.; Mesa, J. L.; Cortes, R.; Villeneuve, G.; Beltran, D. Magnetostructural Correlations in Parallel Square-Planar Halo-Bridged Copper(II) Dimers. Part II: Structure and Magnetic Properties of $[Cu_2(terpy)_2Br_2](PF_6)_2$. *Inorg. Chim. Acta.* **1987**, *134*, 59 – 66.

(51) Rodríguez, M.; Llobet, A.; Corbella, M. A Theoretical Analysis of how Geometrical Distortions on Cu(μ-Cl)$_2$Cu Dimers Influence Their Electronic and Magnetic Properties. *Polyhedron* **2000**, *19*, 2483 – 2491.

For Table of Contents Only

Single crystal ESR experiments reveal unusual anisotropic splitting and merging of lines when crystals rotate in magnetic field. The observation of this partially resolved intradimer dipolar splitting enabled estimation of weak interdimer exchange interaction.